# Assessing aeolian beach-surface dynamics using a remote sensing approach

Irene Delgado-Fernandez[1*], Robin Davidson-Arnott[2], Bernard O.Bauer[3], Ian J. Walker[4], Jeff Ollerhead[5], Hosahng Rhew[6]

[1]Centre for Coastal & Marine Research, School of Environmental Sciences, University of Ulster, Coleraine, UK, BT52 1SA

[2]Department of Geography, University of Guelph, Guelph, ON, Canada, N1G 2W1, rdarnott@uoguelph.ca

[3]Earth & Environmental Sciences and Geography, University of British Columbia, Kelowna, BC, Canada, V1V 1V7, bernard.bauer@ubc.ca

[4]Department of Geography, University of Victoria, Victoria, BC, Canada, V8W 3R4, ijwalker@uvic.ca

[5]Department of Geography & Environment, Mount Allison University, Sackville, NB, Canada, jollerhead@mta.ca

[6]Coastal and Estuarine Morphodynamics Laboratory, Department of Oceanography, INHA University, 253 YongHyun-Dong, Nam-gu, Incheon, 402-751, Korea, rhew0503@hanmail.net

*Present address: Natural, Geographical and Applied Sciences, Edge Hill University, St. Helens Road, Ormskirk, Lancashire, UK, L39 4QP, delgadoi@edgehill.ac.uk

**Abstract**

A remote sensing technique for assessing beach surface moisture was used to provide insight into beach-surface evolution during an aeolian event. An experiment was carried out on October 21, 2007 at Greenwich Dunes, Prince Edward Island National Park, Canada, during which cameras were mounted on a mast on the foredune crest at a height of about 14 m above the beach. Maps of beach surface moisture were created based on a calibrated relationship between surface brightness from the photographs and surface moisture content measured in situ at points spaced every 2.5 metres along a transect using a Delta-T moisture probe. A time sequence of maps of surface moisture content captured beach surface evolution through the transport event at a spatial and temporal resolution that would be difficult to achieve with other sampling techniques such as impedance probes. Erosion of the foreshore and berm crest resulted in an increase in surface moisture content in these areas as the wetter underlying sediments were exposed. Flow expansion downwind of the berm crest led to sand deposition and a consequent decrease in surface moisture content. Remote sensing systems such as the one presented here allow observations of the combined evolution of beach surface moisture, shoreline position, and fetch distances during short-term experiments and hence provide a comprehensive rendering of sediment erosion and transport processes.

***Keywords:*** *beach surface moisture, remote sensing, aeolian geomorphology, Greenwich Dunes*

## 1. Introduction

Surface moisture is an important control on the threshold of movement for aeolian transport and likely on the instantaneous transport rate (Belly, 1964; McKenna Neuman and Nickling, 1989; Namikas and Sherman, 1995; Cornelis and Gabriels, 2003; Wiggs et al., 2004a; Davidson-Arnott et al., 2008; Nordstrom et al., 2011). On beaches, surface moisture can be largely variable over time and space, and it is subject to change during aeolian transport events due to local erosion that exposes underlying wetter sediments or local accumulation of dry sand on a previously wetted surface (e.g. Nield et al., 2011). Until recently, measurements of surface moisture were acquired by taking surface scrapings or cores, and returning the samples to the laboratory for gravimetric analysis. In addition to the considerable labour involved and the difficulty of relating the results to the true moisture content of the surface grain layer itself, this technique resulted in physical disturbance of the surface through sampling and trampling. The development of impedance probes such as the Delta-T Theta probe (Atherton et al., 2001; Wiggs et al., 2004b; Yang and Davidson-Arnott, 2005; Edwards and Namikas, 2009) allowed more frequent measurements of moisture content during transport events, but such probes still have the disadvantage that readings need to be taken at many points and that each measurement integrates moisture over a sampling depth of about 2-6 cm depending on the length of the probe.

The development of remote sensing technologies for assessing surface moisture using the apparent surface brightness offers the potential to sample

73 instantaneously over a substantial area without disturbing the surface, and this
74 approach provides a better measure of the true surface moisture content
75 (McKenna Neuman and Langston, 2006; Darke et al., 2009; Delgado-Fernandez
76 et al., 2009). Remote sensing systems have become increasingly important tools
77 in coastal research, with a number of processes and forms now being monitored
78 using Argus Systems (Holman and Stanley, 2007), satellite imagery (e.g., Wahid,
79 2008), Terrestrial Laser Scanner (TLS; Nield and Wiggs, 2011) and time-lapse
80 photography (e.g., Lynch et al., 2006; Darke et al., 2009; Delgado-Fernandez et
81 al., 2009). Summerfield (2005, p. 403) notes that it is often the introduction of
82 new techniques that stimulates 'leaps of explanatory power' and permits
83 investigation into questions previously discarded as 'incapable of being
84 addressed'. In particular, the deployment of camera systems for periods of
85 months to years has provided rich insight into the nature of aeolian transport
86 events in coastal areas (Delgado-Fernandez and Davidson-Arnott, 2011).

87 The primary purpose of this paper is to discuss the use and potential of a
88 remote-sensing camera system (Delgado-Fernandez et al., 2009) as part of a
89 short-term field experiment designed to measure wind flow and sand transport
90 across a beach foreshore and berm over a period of several hours. In this
91 application imagery was captured every 5 minutes, in contrast to the hourly data
92 collected for the meso-scale monitoring (Delgado-Fernandez, 2011). This
93 allowed detailed assessment of the evolution of surface moisture during the
94 transport event with the prospect of evaluating the effect of moisture on the
95 spatial and temporal variations in the sand transport rate. Information derived

from the remotely sensed imagery was compared to data from the Theta probe in order to determine the accuracy and precision of each methodology. The discussion in this paper focuses on the effects of aeolian transport on surface moisture content rather than moisture as a control on the threshold of aeolian transport. While the latter has been widely discussed, the former can now be investigated by analysing the complexities shown in moisture maps obtained from the remote sensing system.

## 2. Study site

The study site was located at Greenwich Dunes, Prince Edward Island (PEI), Canada (Figure 1). Greenwich Dunes are part of a barrier spit beach-dune complex formed on the east side of the entrance to Saint Peter's Bay, on the north shore of PEI (Mathew et al., 2010). The coast is microtidal with a mixed semidiurnal regime and a maximum range at spring tides of approximately 1 m. The foredune ranges in height from 6 to 10 m with a stoss slope of 20-25° and the dune crest is aligned roughly east-west. The beach is 30-40 m wide and consists predominantly of quartz sand with a mean diameter of 0.26 mm. Marram grass (*Ammophila breviligulata*) covers the foredunes and exhibits considerable seasonal patterns of density and height, with individual plants typically reaching 25 cm heights. The study site was located approximately 1 km east of Saint Peter's Bay, and covered an area of approximately 60 m alongshore. Further information on the study site may be found in Hesp et al. (2005), Walker et al. (2006), Davidson-Arnott et al. (2008) and Bauer et al. (2009).

## 3. Methods

Wind and sand transport intensity

Wind and sand transport were measured using high-frequency instrumentation deployed at five stations set up at 10 m intervals along a transect oriented parallel to the wind direction from the top of the foreshore across the berm crest and upper beach (Figure 2A, B). Wind direction was from the NW at an angle of about 30° from shore parallel. The foreshore was quite gentle with a slope of 2° along the transect and a height difference of about 1.2 m between the berm crest and the low tide terrace (Figure 3B). Station 5 was set up near the upper foreshore, and station 4 was located on the berm crest. Station 3 was located on the gently sloping back surface of the berm crest and station 2 was within a slight dip in the topography that marked the junction between the landward-dipping berm slope and the seaward dipping beach surface on which station 1 was located.

Wind flow was measured using 2-D and 3-D sonic anemometers deployed on H-frames at stations 1 to 4 (Figure 2B). Each station consisted of two Gill 3-D Windmaster sonic anemometers positioned at 0.25 and 1.5 m above the bed, and a Gill 2-D windsonic anemometer mounted at a height of 3 m. These stations were positioned at 0, 10, 20 and 30 m along the profile (Figure 3B). An RM Young cup anemometer was positioned at station 5 near the top of the foreshore slope (40 m) at a height of 0.25 m. A mast with a vertical array of six cup anemometers was positioned near the back of the beach, but the data are not utilised in this paper.

142 Sand transport intensity was measured using two different sensor types:
143 'Safire' piezoelectric impact sensors (Baas, 2004; Barchyn and Hugenholtz, 2010)
144 and Wenglor laser sensors (Davidson-Arnott et al., 2009; Hugenholtz and
145 Barchyn, 2011). The Safires count only grains with sufficient momentum to
146 register when they strike the 2 cm sensing ring, and grains that are too small, too
147 slowly moving, or which only graze the sensor are not registered as counts. The
148 sensitivity of the sensor also varies around the circumference of the instrument,
149 particularly away from the two 'sweet spots' that mark the point of attachment of
150 the leads to the sensing ring (Baas, 2004). It has been shown that the sensitivity
151 varies from one sensor to another, and that sensitivity will vary over time
152 particularly as the rubber sheathing weathers. The five Safires deployed here
153 were selected after tests in the laboratory showed that their response to varying
154 rates of sediment discharge in an air fall column was very similar. The
155 instruments were deployed with their 'sweet spot' facing directly into the wind,
156 thus removing concerns of directionality.
157 The laser sensor (Wenglor® model YH03PCT3) consists of a laser and
158 photo sensor mounted within a U shaped frame with a spacing (path length) of 3
159 cm and a beam diameter of 0.6 mm. The instrument detects the drop in voltage
160 at the photo sensor resulting from the passage of individual grains through the
161 beam. The counting circuitry is contained within the instrument and is capable of
162 detecting >2000 grains per second. Evaluation of the sensors indicates that they
163 count all grains (or portions of grains) above the cut-off size that pass through the
164 beam, irrespective of speed. As with all such sensors, they cannot distinguish

between particles entering the beam at exactly the same time so that a few particles are missed at moderate transport rates. At very large transport rates the actual count may go down (Hugenholtz and Barchyn, 2011) but this only occurs during very intense transport events. Transport rates here were never extreme enough for the latter to be a consideration (Davidson-Arnott et al., 2009).

Safires were deployed at all five stations but the sensor at station 4 failed early in the experiment. Wenglor laser sensors were deployed at stations 2 and 3 and also at a point half way between stations 1 and 2 (identified here as station 1.5). All sensors were sampled at 1 Hz over the course of the experiment. Because of capacity restrictions the data logger at station 5 had to be downloaded part way through the experiment resulting in a gap in data collection from the anemometer and Safire at that station. There was considerable noise in the data recorded by the anemometer at a height of 0.25 m at station 4 and, while it was possible to remove some of this through filtering, the uncertainties introduced into calculations of five-minute means meant that data from this sensor were discarded. Finally, sand transport rates were measured using vertical V traps (Nickling and McKenna Neuman, 1997) during four runs with a duration of 20 minutes (run 1) and 15 minutes (runs 2-4).

Moisture content and image processing

The long-term monitoring station at Greenwich consisted of three digital SLR cameras operated by a timer that triggered exposures every hour from May 2007 to May, 2010. The cameras were deployed on top of a 6 m mast located on

top of the 8 m high foredune crest (Figure 2C). The west camera had a field of view of approximately 100 m; the north camera covered a field of view of approximately 40 m alongshore; and the east camera covered an alongshore distance of 1.5 km. The east camera provided qualitative data on beach and weather conditions but the west and north cameras were used to extract numerical information such as moisture maps (MM) or fetch distances (Delgado-Fernandez et al., 2009). The short-term experiment described in this paper was conducted over a period of about six hours on October 21, 2007 within the field of view of the north camera (Figure 3A). Cameras were set to take exposures every five minutes during the short-term experiment.

The camera images were used to obtain time series of a number of key factors affecting aeolian sediment transport, such as moisture content and fetch distances (Delgado-Fernandez, 2011). In particular moisture maps (MM) were created by an automatic process (using Geomatica v9.1-Easi scripts) involving moisture calibration, image rectification and establishment of spatial extent and resolution. The process is described in detail by Delgado-Fernandez et al. (2009).

Moisture calibration consists of correlating surface brightness recorded by digital cameras with moisture content measured at the beach surface (Darke et al., 2009). Digital sampling of pixel brightness was conducted at beach locations where moisture samples were collected through surface scraping. Pixel brightness values were normalized against the brightness value of a ‘white board’ in order to compensate for the effect of different environmental light in the exposures due to sun angle and weather conditions. A calibration curve was

obtained by plotting normalized brightness against percent moisture content obtained from laboratory analysis, which allowed subsequent calculation of moisture values from pixel brightness values (Delgado-Fernandez et al., 2009). Image rectification transformed oblique imagery into georeferenced data by matching ground control points deployed within the field of view of the cameras with their corresponding map coordinates (surveyed with differential global positioning system). The raster cell size of the output rectified maps was 0.05 m and was set during the process of image rectification. This was the finest resolution possible given the area covered by an original pixel located in the farthest position (relative to the camera) subject to rectification. Shoreline position was digitized for each MM and vegetation cover was extracted using unsupervised classifications (Delgado-Fernandez et al., 2009). This allowed delimiting the beach width, which was used to establish the spatial extent of the MM.

Finally, near-surface moisture content was measured with a Delta-T Theta probe along the instrument transect at 2.5 m intervals. Sampling points were marked with rods (Figures 2B and 3) that were visible within the images taken by the camera. The probe was systematically used on the landward side of the rod, which allowed subsequent comparison between moisture values obtained with the Theta-probe and moisture values digitally sampled at the same locations in the corresponding MM (section 4). Moisture measurements were taken before runs 1-3 and after run 4 of the trap runs, at approximately 62, 112, 190 and 242 minutes from the start of the experiment. The length of the stainless steel rods of

234 the probe was shortened from the original 6 cm to 2 cm by using a 4 cm thick
235 dielectric foam (Yang and Davidson-Arnott, 2005).
236
237 **4. Results**
238 Spatio-temporal variations in wind flow and sediment transport intensity
239 Wind speed averaged over five-minute periods are plotted in Figure 4A
240 from the start of the experiment at 09:43 until 13:53 (250 minutes later) when
241 recording ceased for the anemometers at stations 5, 3, 2 and 1. The general
242 pattern recorded at all four stations was similar, with largest speeds recorded at
243 station 5 near the top of the foreshore slope. There was an initial increase in
244 mean speed to about 8.5 $ms^{-1}$ at station 5 about 15 minutes after the start of
245 recording followed by a decrease to about 7.3 $ms^{-1}$. After 60 minutes the speed
246 increased again, reaching a peak of approximately 9.5 $ms^{-1}$ at about 90 minutes,
247 remaining steady at this speed until 120 minutes and then decreasing to 8 $ms^{-1}$
248 by 160 minutes. The corresponding averages for transport intensity are plotted
249 for the four safires in Figure 4B and for the three Wenglor laser probes in Figure
250 4C. The temporal variations in mean sand transport intensity were somewhat
251 more complex than for winds but showed a similar pattern with a peak early in
252 the measurement period followed by a period with very low values for transport
253 intensity and then much larger values between 90 and 120 minutes. This was
254 followed by decreasing values until the end of the experiment, with the exception
255 of the Wenglor at station 3, which showed more variability.

256 The spatial pattern of wind speed across the profile can be seen more
257 clearly by comparing plots of five-minute means for five intervals (Figure 5B) that
258 are representative of the range of conditions over the recording period, with the
259 profile along the instrument line (Figure 5A). Except at the very end of the
260 recording period the wind speed pattern showed largest speeds at station 5 near
261 the top of the foreshore slope, slightly lower speeds at station 3 near the back of
262 the berm crest and a further reduction in speed at station 2 located in the shallow
263 dip of a remnant runnel at the landward end of the berm. Wind speed increased
264 slightly at station 1 on the back beach. The pattern was consistent with
265 acceleration due to flow compression as the wind traveled obliquely across the
266 foreshore slope and then a small deceleration due to flow expansion in the lee of
267 the berm crest. Unfortunately because of the problems with the lowermost sonic
268 anemometer at station 4 it was not possible to determine if there was flow
269 separation, but there is no consistent evidence for this in the records at station 3
270 and, because of the modest relief and relatively gentle apparent slope of the
271 oblique transect, it seems likely that flow remained attached over this distance.
272 The largest transport intensity measured by the safires was generally
273 found at station 3, landward of the berm crest, followed closely by the probe at
274 station 5 (Figure 5C). Smaller values were recorded at stations 1 and 2; however,
275 values for transport intensity at station 1 were almost always larger than those for
276 station 2. The largest values for the Wenglor laser sensors were also recorded at
277 station 3, with the smallest values recorded at station 2 and somewhat larger
278 values at the probe located between stations 2 and 1 (station 1.5). This shows

279 that similar spatial patterns of sand transport intensity were recorded by these
280 two different sensor types.

281 Actual sand transport rates were measured using vertical integrating traps
282 that were deployed at all five stations. The trap data thus permit some evaluation
283 of transport conditions at station 4 compared to those at stations 5 and 3 (Figure
284 5D). Transport rates at station 4 on the berm crest were always larger than at
285 station 5. This pattern is to be expected if we assume that wind speed was likely
286 somewhat larger here because of flow acceleration due to flow compression up
287 the foreshore slope. Transport rates might also be expected to increase across
288 the profile with increasing fetch and decreasing surface moisture content.
289 Transport rates at station 4 were also larger than at station 3 except at the very
290 end of the experiment when wind speed had decreased considerably. At this time
291 it would be expected that the combination of light winds and larg surface moisture
292 on the foreshore slope would result in conditions that were below the threshold
293 for much of the time at this location, and transport would be largely confined to
294 entrainment of dry sand from the surface of the berm and backshore.

295

296 Spatio-temporal variations in surface moisture

297 Images of the beach were acquired every five minutes, which resulted in a
298 total of 50 MM. An examination of the moisture conditions at this frequency
299 revealed that changes were difficult to discern, and hence, 30-minute time
300 intervals were used to asses changes in surface moisture (Figure 6A). A
301 representative sample corresponding to the middle period of the experiment is

302 shown here, from approximately 10:30 (55 min) to 13:00 (205 min). In addition to
303 the moisture maps themselves, difference maps were generated by subtracting
304 the data for each raster in one time period from the data for the same raster in
305 the previous time period (Figure 6B). Three classes of surface moisture change
306 were utilised: no change, drier, and wetter, with the last two classes
307 corresponding to a decrease or increase in moisture content > 2% respectively.
308 The surface at the end of the first hour was slightly damp, ranging from 2 to 6%
309 moisture content. A gradual increase in near-surface wind speed from 50 to 100
310 minutes (Figure 4A) led to erosion of a surficial layer of dry sand from the
311 foreshore resulting in the west area beach surface becoming wetter at 85
312 minutes (Figure 6A). Wind speed continued to increase up to 115 minutes and
313 remained steady and relatively strong until approximately 125 minutes. MM from
314 85 minutes to 145 minutes show a surface that progressively became drier on the
315 backshore (due to deposition of dry sand) but especially wetter on the foreshore
316 and west area (due to progressive erosion), as shown in the maps of changes in
317 moisture content (Figure 6B). In contrast with the first part of the experiment, the
318 foreshore became gradually dryer at 175 and especially at 205 minutes, with the
319 formation of a continuous patch of dry sediment in front of all stations. This was
320 due to a combination of sunnier conditions favouring evaporation across the
321 beach surface and relatively gentle winds not capable of eroding the newly dried
322 sand in the foreshore.

323 Moisture measurements with the Theta probe (Fig 7B) showed relatively
324 small moisture content (5-7%) across the backshore, increasing moisture at the

325 berm and upper foreshore (6-8%), and the largest moisture content on the lower
326 foreshore (9-12%). Moisture content was also re-sampled using the digital MM
327 for the same locations at two grid resolutions: 0.05 m (Figure 7C) and 0.5 m
328 (Figure 7D). The latter were created through a process of image coarsening,
329 which combines cells into a larger cell and averages the values of the cells
330 contained within it (Woodcock and Strahler, 1987). In the example used here,
331 each 0.5 m cell represents the average of 100 0.05 m cells. The trends obtained
332 from the MM followed, in general terms, those identified with the Theta probe.
333 However the readings obtained from the coarser resolution maps (Figure 7D)
334 showed simpler trend patterns, while moisture values sampled from the finest
335 resolution maps (Figure 7C) showed unrealistically large variability. Average
336 values from the 0.5 m renditions were therefore adopted for the purpose of
337 comparison to the Theta probe values. Figure 8 shows a comparison of moisture
338 content values obtained from the Theta probe along the profile versus those
339 obtained from MM at 0.5 m grid resolution for different time intervals. In general,
340 moisture values obtained from MM presented larger variability, with both drier
341 and wetter zones than those obtained from the Theta probe. The remote sensing
342 images seem highly sensitive to slight wetting or drying of the surface while this
343 does not show up in the Theta probe results. Note that moisture readings taken
344 close to the east side of the image (e.g., 15 m) at 112 minutes were greater than
345 what would be expected from a dry surface. These are currently being explored
346 as they could be a product of inaccuracies of moisture values at the edges of the

MM or a product of slight drizzle earlier in the morning, since they are no longer visible later in the day (see following section).

Co-evolution of surface moisture and sediment transport

Figure 9 shows time series for wind direction, wind speed, fetch distance, moisture content obtained from the 0.5 m grid resolution MM, and transport intensity given by the Safires for stations 1-5. Wind direction and speed data are from the 2-D sonic at a height of 3 m at station 4 and are used to provide general information of the incident wind field since this should be unaffected by growth of the boundary layer associated with compression of flow up the foreshore slope. Gaps in the moisture and fetch graphs correspond to periods of time when no images were taken. Wind direction was initially very constant, from approximately 10° to the E of the instrument transect (aligned with a wind direction of 180°), gradually becoming more onshore (where directly onshore is 270$^{o}$) and staying at 20° to the E of the instrument transect by the end of the experiment. Figure 3C shows the approximate location of the shoreline at the beginning and end of the experiment, with small changes at this particular location. However, the combined effect of a rising tide and gradual change in wind direction resulted in a decrease of available fetch distance towards the end of the experiment, especially in the landward stations because of differences in beach configuration (see DEM of Figure 3A). The fetch distance decreased over the course of the experiment by 9 m at station 5 and 22 m at station 1 (Figure 9). This reduced fetch has significant implications for sediment transport potential across the

beach and may explain, in part, why transport intensity after about 140 minutes was greatly reduced (Fig 9E).

The beginning of the experiment was marked by cloudy conditions and occasionally light drizzle, which when combined with relatively calm wind conditions may have played a role in the reduction in sand transport during the first hour. The drizzle ended about 50 minutes into the experiment, and soon after that the clouds cleared so that evaporation due to solar radiation became a factor in the reduction of surface moisture content during the latter half of the experiment. Increased sediment transport during the second hour likely reflects both increasing wind speed and surface evaporation. Note that while this is the trend at stations 4 and 3 (Figure 9D), station 5 (closer to the foreshore) was characterised by increasing surface moisture content due to progressive stripping of the dry surface sediment and exposure of the wetter materials below.

The foreshore and lower beach were erosion zones whereas the back beach was a deposition zone. At the end of the transport event, measurements showed that about 5 cm of scour had occurred at station 5 with a smaller amount at station 4 on the berm crest (Figure 10A). In contrast about 5 cm of deposition was measured at station 3, 3 cm at station 2, and about 1 cm at station 1 (Figure 10B). The configuration of this spatial zonation from shoreline to the foredune toe became gradually aligned normal to the incoming wind direction as the event progressed, with a transition zone in between strongly affected by beach topography and shoreline position. The transition zone was a relatively wide area (roughly around station 4) with a mixture of moist and dry conditions, and

393 characterized by a fairly corrugated edge line resulting from transport processes
394 acting on a very complex surface due to the presence of stones, flotsam, and
395 footprints characterising the erosional surface (Figures 6 and 10C). This level of
396 complexity favours spatial approaches such as MM and remotely sensed data
397 over spot measurements along single transects such as those collected from
398 Theta-T probes, which do not provide enough detail on spatial textures.
399
400 **5. Discussion**
401 Comparison of Theta-T and MM moisture values raise a number of
402 questions regarding the assessment of surface moisture content as a primary
403 control on aeolian sediment transport. Values from MM of 0.5 m resolution
404 showed a better correlation with the Theta-T probe values, which are reliable
405 indicators of surface moisture content when there are smooth transitions in
406 moisture gradients along a given beach transect. Values from MM at 0.05 m
407 resolution contain a large degree of variability in moisture readings, and the
408 question is whether such variation is ‘noise’ or a true representation of the nature
409 of the evolving beach surface during a transport event. When transport was
410 active, there were discrete zones of dry sand that were being deposited beside a
411 moist transport surface that was recently eroded. For example, Figure 2B shows
412 a complex surface with moisture patches alongside dry sand as a result of active
413 aeolian streamers and deposition/erosion processes. In this instance, the MM
414 appear to be yielding ‘noisy’ but detailed information that may be representative
415 of the complex evolution of the beach surface through time. Further analysis is

being undertaken to investigate these micro-scale complexities and to assess the accuracy of moisture data at the edges of MM.

A related issue has to do with quantifying a characteristic moisture value that should be used in explanations of sediment transport as a function of wind, moisture, and fetch distances. The 0.05 m resolution MM provide detailed representations of beach surface moisture but sediment transport rates might correlate better with averaged moisture values over a given area. Furthermore, transport rates could be better explained using some measure of the spatial distribution of moisture values over a set distance (e.g., 1 m, 2 m, or 10 m) in front of a given trap. MM provide an excellent platform for these types of investigations because they allow analysis of moisture content at different spatial resolutions.

In addition to providing a measure of the actual moisture content of the upper-most sand grain layer, in contrast to the depth-averaged sample (from 1.5-6 cm thickness) from the Theta probe (Atherton et al., 2001; Yang and Davidson-Arnott, 2005; Schmutz and Namikas, 2011), the process of cell aggregation of fine resolution (0.05 m) MM into coarser resolution (0.5 m) MM offers the advantage of providing more representative spatially-average values. Detailed sampling of surfaces with moderate moisture content using the Theta probe have shown that there can be a large degree of variability within an area as small as 1 $m^2$ (Yang and Davidson-Arnott, 2005; Edwards and Namikas, 2009). While Theta probes provide point measurements that are assumed to be representative of a given area, a cell from the coarse resolution MM presented here would represent

439 the average of 100 moisture measurements over an area of 0.5 $m^2$. Taking a
440 similar size sample with a Theta probe would be intrusive and obviously highly
441 time consuming.

442 While surface moisture is an important control on aeolian transport (Belly,
443 1964; McKenna Neuman and Nickling, 1989; Namikas and Sherman, 1995;
444 Cornelis and Gabriels, 2003; Wiggs et al., 2004b; Davidson-Arnott et al., 2008)
445 results from this study demonstrate that transport is in turn an important control
446 on surface moisture content as the beach surface evolves through localized
447 erosion and deposition. Surface moisture is related to transport in two opposing
448 ways. Safires at stations 5 (foreshore) and 3 (back beach) recorded a peak of
449 transport intensity from approximately 80 to 120 minutes, coinciding with the
450 increase of wind speed. However, surficial moisture content increased at station
451 5 but decreased at station 3 (Figure 9). The combination of flow acceleration up
452 the foreshore slope and a short fetch (no sediment source upwind) transformed
453 the foreshore (station 5) into an erosive zone. Hence, relatively large values for
454 moisture content at this location were the result of sediment erosion and
455 landward transport. This is in line with observations on sediment transport
456 dynamics on a drying beach by Nield et al. (2011) who reported erosion of dry
457 sediment leading to an increase of surface moisture due to the exposure of the
458 underlying, wetter surface. Large transport rates at station 3 (back beach) were
459 associated with significant accumulation of dry sand and hence small values of
460 surface moisture content. Details of the temporal evolution of moisture content in
461 these two different zones reveal complex feedbacks between moisture, wind

speed, sand transport, and fetch distances where moisture is not only a control for sediment movement but also a result of patterns of erosion and accumulation. The largest transport rates at stations 5 and 3 were recorded during the first trap run (96 minutes; Figure 5D), coinciding with the strongest wind speeds and the peak of saltation recorded by the Safires (Figure 9). As suggested by the MM (Figure 6A) most of the sand collected during this run at station 5 was the result of the erosion of a relatively dry layer from the foreshore, which in turn increased the surface moisture content there. Transport rates at station 5 during the second run (127 minutes) were smaller than at station 1 (Figure 5D) despite strong winds of 9-9.5 $ms^{-1}$ similar to those recorded during run 1. Hence the erosion of the layer of dry sediment from this zone during run 1 produced larger levels of surface moisture during run 2, which in turn limited further erosion. At stations 3-1, dry sediment stripped from the foreshore was deposited progressively leading to drier surface sediment. These deposits are easily mobilized under stronger wind conditions, but boundary layer evolution leads to reduced surface shear stress and hence, deposition toward the toe of the dune.

## 6. Conclusion

This paper demonstrates the applicability of a remote sensing system to measuring beach surface moisture over a short-term experiment. The detailed temporal and spatial resolution of the evolution of surface moisture provided by the time-lapse photography provides an improved explanation for the spatial and temporal patterns of sand transport, and the changes in the beach surface

485 resulting from scour and deposition. The conclusions can be summarised as
486 follows:

487 1) Spatial patterns of erosion, transport and deposition over the foreshore
488 and berm reflect the changing boundary layer produced by flow
489 compression up the foreshore slope and then expansion over the reverse
490 slope on the landward side of the berm;

491 2) Temporal patterns of sand transport intensity reflect both changes in wind
492 speed and direction (fetch distance) over the event, upwind sources of
493 available dry sediment, and the effects of changes in surface moisture;

494 3) Fine resolution moisture maps offer the possibility of data aggregation
495 through pixel coarsening and may be used to explore appropriate moisture
496 values for different applications. While averaged moisture values obtained
497 from coarser resolution (0.5 m) MM were more similar to those obtained
498 with the Theta probe these may be smoothing out important micro-scale
499 information. Further research should be conducted to determine the
500 appropriate temporal and spatial resolution of moisture measurements.

501 4) The high resolution of the surface MM permits the identification of changes
502 in moisture over the whole surface that reflect external conditions such as
503 solar radiation input and precipitation as well as internal conditions
504 produced by the erosion (wetting) and deposition (drying) of sand.

505 5) The remote sensing system thus provides a relatively simple approach to
506 measuring the evolution of the beach surface during a transport event, and

to providing more comprehensive explanations of processes of erosion and transport and changes in surface conditions.

**Acknowledgements**

We thank Parks Canada for granting permission to carry out work at Greenwich Dunes and personnel at Greenwich Dunes for their support in the field, especially Kirby Tulk, Allan Doyle, Tarah McFee, Roger Steadman, and Miguel Santos. Rosie Smith conducted the DGPS surveys, Mario Finoro and Sandy McLean provided technical support with building and testing equipment, and Adam Bonnycastle aided in the development of scripts. Financial support was provided through a Natural Sciences and Engineering Research Council of Canada Discovery Grant to RD-A, through a research grant from Parks Canada to RD-A, IJW and JO, and through the Ontario Graduate Scholarship Program and University of Guelph Lattornell Travel grant to ID-F.

**References**

Atherton R.J, Baird, AJ, Wiggs GFS. 2001. Inter-tidal dynamics of surface moisture content on a meso-tidal beach. Journal of Coastal Research **17** : 482-489.

Baas AC W. 2004. Evaluation of saltation flux impact responders (Safires) for measuring instantaneous aeolian sand transport intensity. Geomorphology **59** : 99-118.

529 Barchyn TE, Hugenholtz CH. 2010. Field comparison of four piezoelectric
530 sensors for detecting aeolian sediment transport. Geomorphology **120** :
531 368-371.
532 Bauer BO, Davidson-Arnott RGD, Hesp PA, Namikas SL, Ollerhead J, Walker IJ.
533 2009. Aeolian sediment transport on a beach: surface moisture, wind fetch,
534 and mean transport. Geomorphology **105** : 106–116.
535 Belly PY. 1964. Sand movement by wind. U.S. Army Corps of Engineers CERC,
536 Tech. Memo. 1 : 38 pp.
537 Cornelis WM, Gabriels D. 2003. The effect of surface moisture on the
538 entrainment of dune sand by wind: an evaluation of selected models.
539 Sedimentology **50** : 771-790.
540 Darke I, Davidson-Arnott RGD, Ollerhead J. 2009. Measurement of Beach
541 Surface Moisture Using Surface Brightness. Journal of Coastal Research
542 **26** : 248-256.
543 Davidson-Arnott RGD, Yang Y, Ollerhead J, Hesp PA, Walker IJ. 2008. The
544 effects of surface moisture on aeolian sediment transport threshold and
545 mass flux on a beach. Earth Surface Processes and Landforms **33** : 55–74.
546 Davidson-Arnott RGD, Bauer BO, Walker IJ, Hesp PA, Ollerhead J, Delgado-
547 Fernández I. 2009. Instantaneous and mean aeolian sediment transport
548 rate on beaches: an intercomparison of measurements from several
549 sensor types. *Journal of Coastal Research*, SI 56, 297-301.

550 Delgado-Fernandez I, Davidson-Arnott RGD, Ollerhead J. 2009. Application of a
551 remote sensing technique to the study of coastal dunes. Journal of
552 Coastal Research **25** : 1160–1167.
553 Delgado-Fernandez I. 2011. Meso-scale modelling of aeolian sediment input to
554 coastal dunes. Geomorphology **130** : 230-243.
555 Delgado-Fernandez I, Davidson-Arnott RGD. 2011. Meso-scale aeolian sediment
556 input to coastal dunes: The nature of Aeolian transport events.
557 Geomorphology **126** : 217–232
558 Edwards BL, Namikas SL. 2009. Small-scale variability in surface moisture on a
559 fine-grained beach: implications for modeling aeolian transport. Earth
560 Surface Processes and Landforms **34** : 1333-1338.
561 Hesp PA, Davidson-Arnott RGD, Walker IJ, Ollerhead J. 2005. Flow dynamics
562 over a foredune at Prince Edward Island, Canada. Geomorphology **65** :
563 71-84.
564 Holman RA, Stanley J. 2007. The history and technical capabilities of Argus.
565 Coastal Engeenering Reseach Centre **54** : 477-491.
566 Hugenholtz CH, Barchyn TE. 2011. Laboratory and field performance of a laser
567 particle counter for measuring aeolian sand transport. Journal of
568 Geophysical Research. **116** : F01010, 13 pp. doi:10.1029/2010JF001822
569 Lynch K, Jackson DWT, Cooper AG. 2006. A remote-sensing technique for the
570 indentification of aeolian fetch distance. Sedimentology **53** : 1381-1390.
571 Mathew S, Davidson-Arnott RGD, Ollerhead J. 2010. Evolution of a beach–dune
572 system following a catastrophic storm overwash event: Greenwich Dunes,

573 Prince Edward Island, 1936–2005. Canadian Journal of Earth Science. **47**
574 : 1–18
575 McKenna Neuman C, Nickling WG. 1989. A theoretical and wind tunnel
576 investigation of the effects of capillary water on the entrainment of
577 sediment by wind. Canadian Journal of Soil Science **69** : 79-96.
578 McKenna Neuman C, Langston G. 2006. Measurement of water content as a
579 control of particle entrainment by wind. Earth Surface Processes and
580 Landforms **31** : 303–317.
581 Namikas SL, Sherman DJ. 1995. A review of the effects of surface moisture
582 content on aeolian sand transport. Desert Aeolian Processes. V. P.
583 Tchakerian. London, Chapman and Hall Ltd **:** 269-293.
584 Nickling WG, McKenna Neuman C. 1997. Wind tunnel evaluation of a wedge-
585 shaped aeolian transport trap. Geomorphology **18** : 333-345.
586 Nield JM, Wiggs GFS. 2011. The application of terrestrial laser scanning to
587 aeolian saltation cloud measurement and its response to changing surface
588 moisture. Earth Surface Processes and Landforms **36** : 273–278.
589 Nield JM, Wiggs GFS, Squirrell RS. 2011. Aeolian sand strip mobility and
590 protodune development on a drying beach: examining surface moisture
591 and surface roughness patterns measured by terrestrial laser scanning.
592 Earth Surface Processes and Landforms 36 : 513–522.
593 Nordstrom KF, Jackson NL, Korotky KH, Puleo JA. 2011. Aeolian transport rates
594 across raked and unraked beaches on a developed coast. Earth Surface
595 Processes and Landforms 36 : 779–789.

596 Schmutz PP, Namikas SL. 2011. Utility of Delta-T Theta probe for obtaining
597 surface moisture measurements from beaches. Journal of Coastal
598 Research **27** : 478-484.
599 Summerfield MA. 2005. The changing landscape of geomorphology. Earth
600 Surface Processes and Landforms **30** : 779-81.
601 Wahid AM. 2008. GIS-Based Modeling of Wind-Transported Sand on the Qaa
602 Plain Beach .Southwestern Sinai. Egypt. Journal of Coastal Research **24** :
603 936-943.
604 Walker IJ, Hesp PA, Davidson-Arnott RGD, Ollerhead J. 2006. Topographic
605 Steering of Alongshore Airflow over a Vegetated Foredune: Greenwich
606 Dunes, Prince Edward Island, Canada. Journal of Coastal Research **22** :
607 1278-1291.
608 Wiggs GFS, Baird AJ, Atherton RJ. 2004a. The dynamic effects of moisture on
609 the entrainment and transport of sand by wind. Geomorphology **59** : 13–30.
610 Wiggs GFS, Atherton RJ, Baird AJ. 2004b. Thresholds of aeolian sand transport:
611 establishing suitable values. Sedimentology **51** : 95–108.
612 Woodcock CE, Strahler AH. 1987. The factor of scale in remote sensing. Remote
613 Sensing of Environment **21** : 311-332.
614 Yang Y, Davidson-Arnott RGD. 2005. Rapid measurement of surface moisture
615 content on a beach. Journal of Coastal Research **21** : 447–452.
616
617
618

619 **List of Figures**

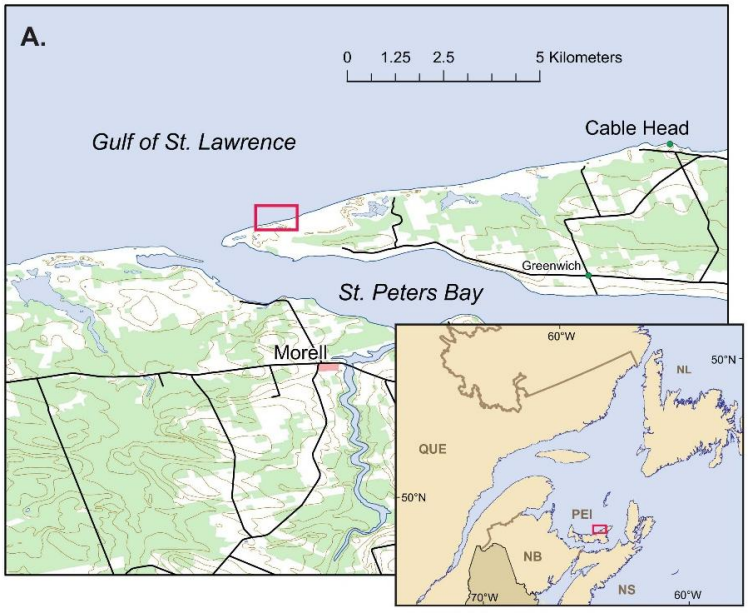


Figure 1: Location of study site at Greenwich Dunes, Prince Edward Island (Canada).

620

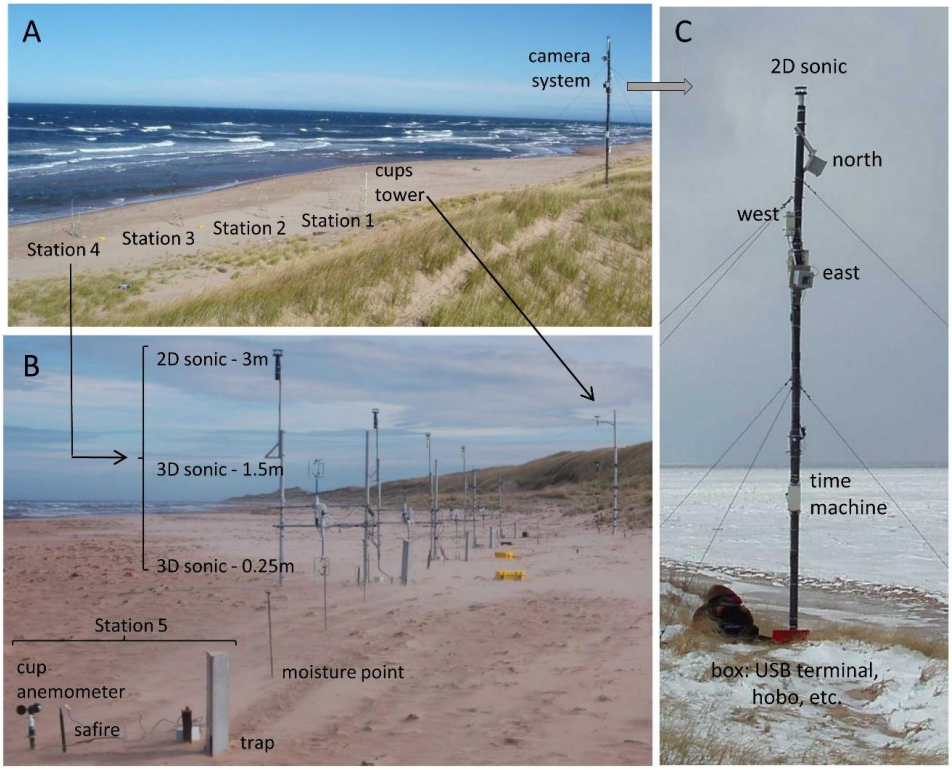


Figure 2: A) General view of study site and instruments; B) close-up of instruments setup. The transect consisted of four stations, each with one 2D and two 3D sonic anemometers located at 3, 1.5, and 0.25 m over the beach surface, and one station with a cup anemometer at 0.25 m over the beach surface. Traps and safires were co-located at each of the stations and moisture points selected every 2.5 m. The transect ran into the incoming wind direction (oblique onshore) and ended in a tower of cup anemometers close to station 1; C) close-up of camera system.

621

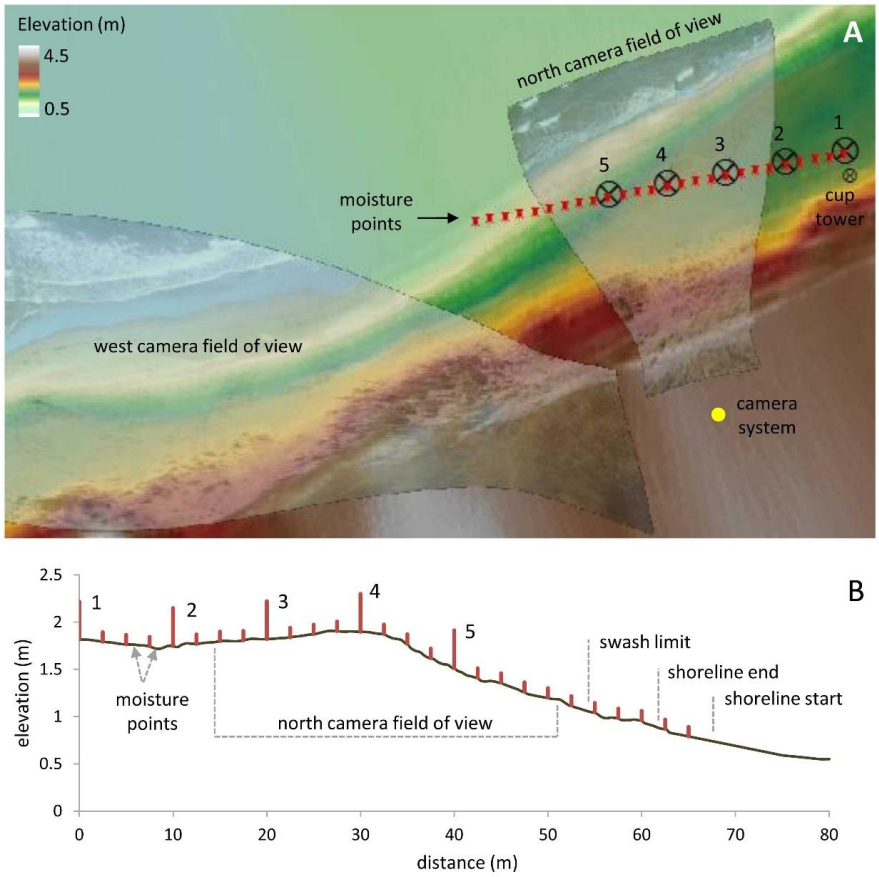


Figure 3: A) Digital elevation model (DEM) georectified from 1 m spot resolution differential global positioning system (DGPS) data. Topographic data was gathered on the beach surface and up to the dune toe and thus the DEM does not include the dune. The position of each station is marked with the station number. Stations 3-5 and a total of 15 moisture points were within the north camera field of view (inserted as a semi-transparent image); B) topographic profile along the instruments transect, showing the approximate location of the shoreline position at the beginning (shoreline start) and end of the experiment.

622

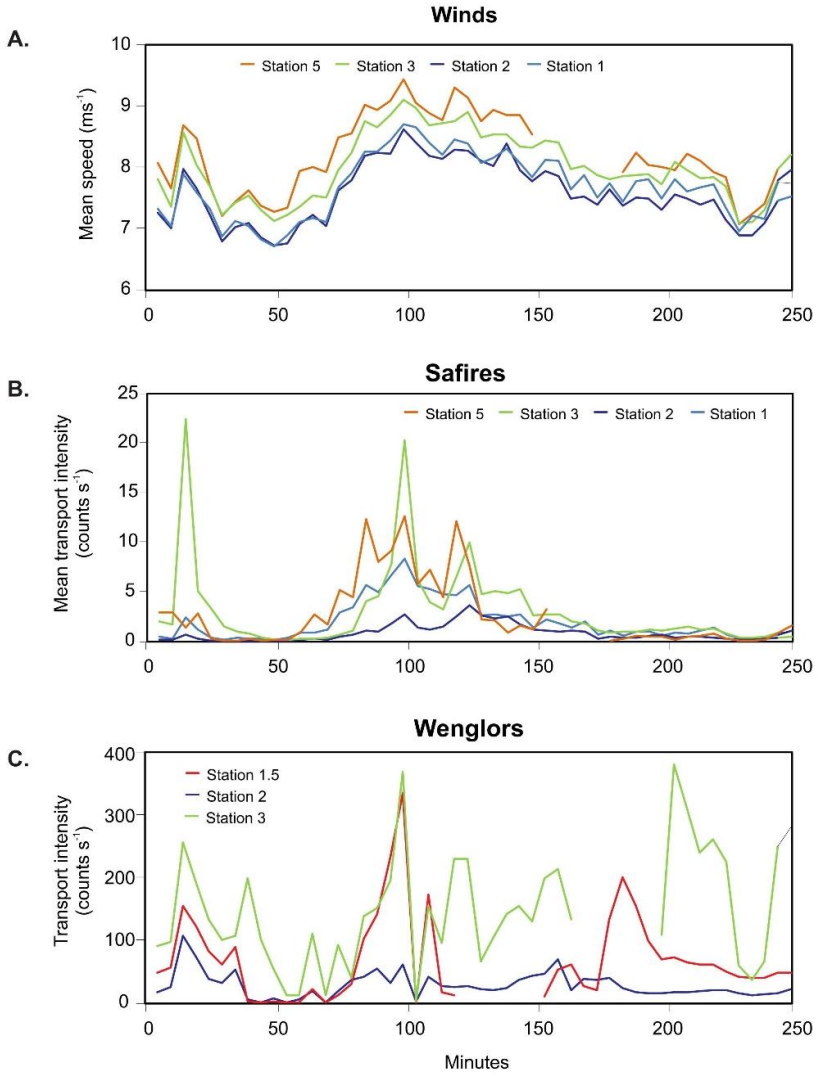


Figure 4: Temporal variations in wind speed and sediment transport intensity. A) five-minute averages for wind speed ($ms^{-1}$) measured at stations 1, 2, 3 and 5 at 0.25 m height; B) average saltation intensity (counts $s^{-1}$) measured by Safire probes at the same stations; C) average saltation intensity (counts $s^{-1}$) measured by Wenglor laser sensors at stations 2, 3 and midway between 1 and 2. Note that the grain counts measured by the Wenglors are much larger than those measured by the Safires (see Davidson-Arnott et al., 2009).

623

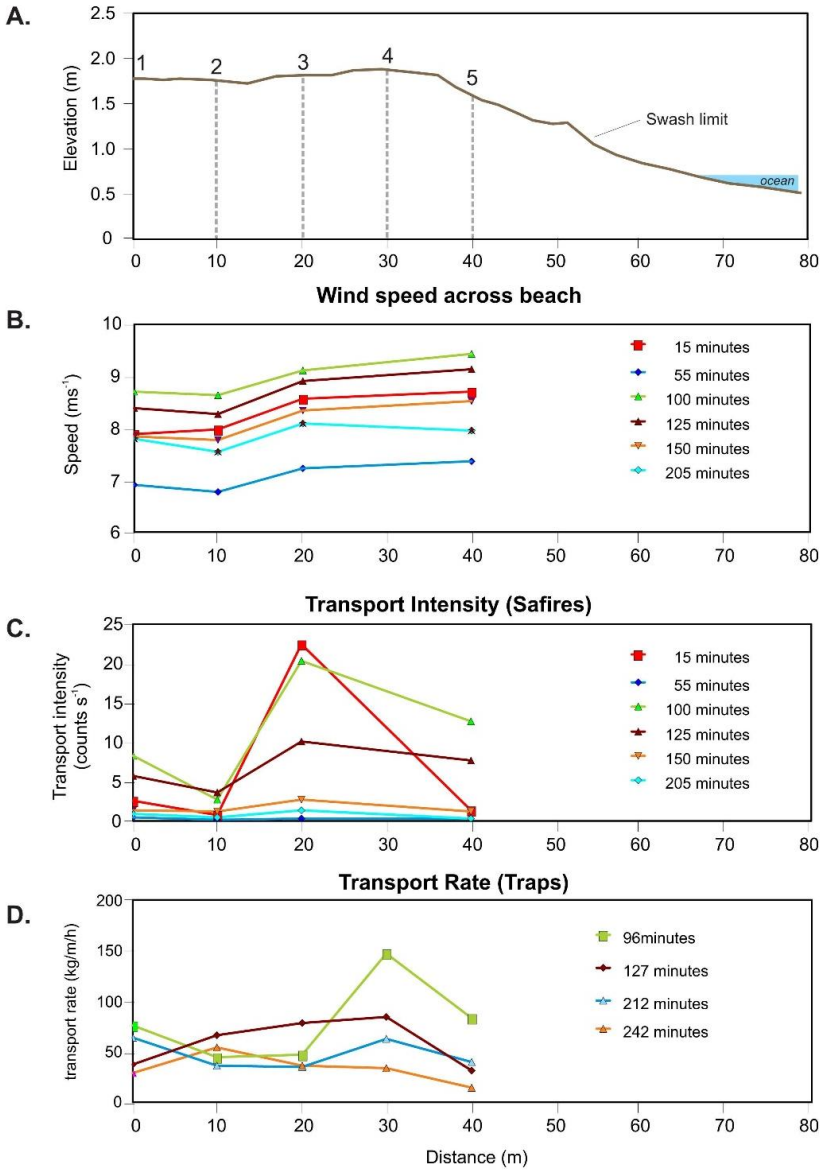


Figure 5: Spatial pattern of winds and sediment transport. A) beach profile along instruments transect; B) mean wind speeds for 6 five minute periods; C) transport intensity measured by the Safire probes for the same 5 minute periods as B); D) transport rate measured by vertical traps. Run 1 had a duration of 20 minutes and the other thre runs a duration of 15 minutes. Times are for the end of the run.

624

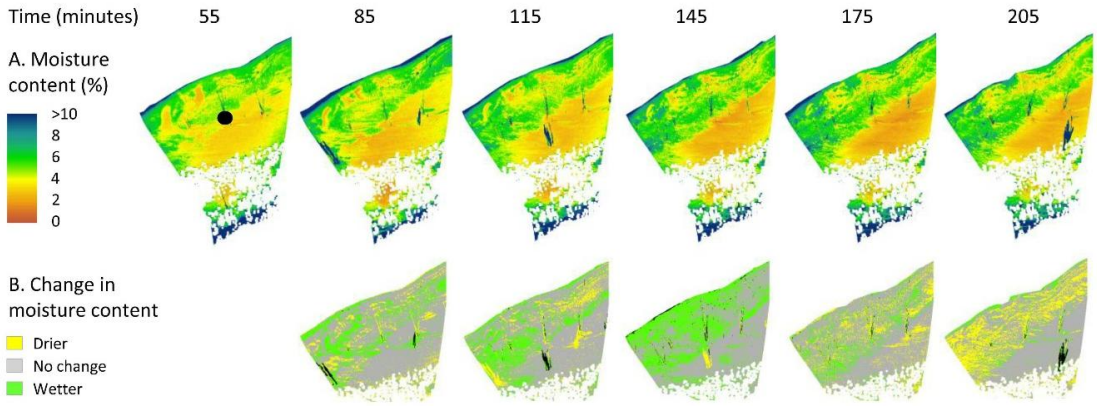


Figure 6: Temporal variations in moisture content. A) temporal sequence of moisture maps every 30 minutes; B) maps showing the change in moisture content relative to the previous moisture map. Only relative changes over +/-2% have been considered, with drier areas (change > 2%) shown in orange and wetter areas (changes > -2%) in green. The black dot shows the location of station 4.

625

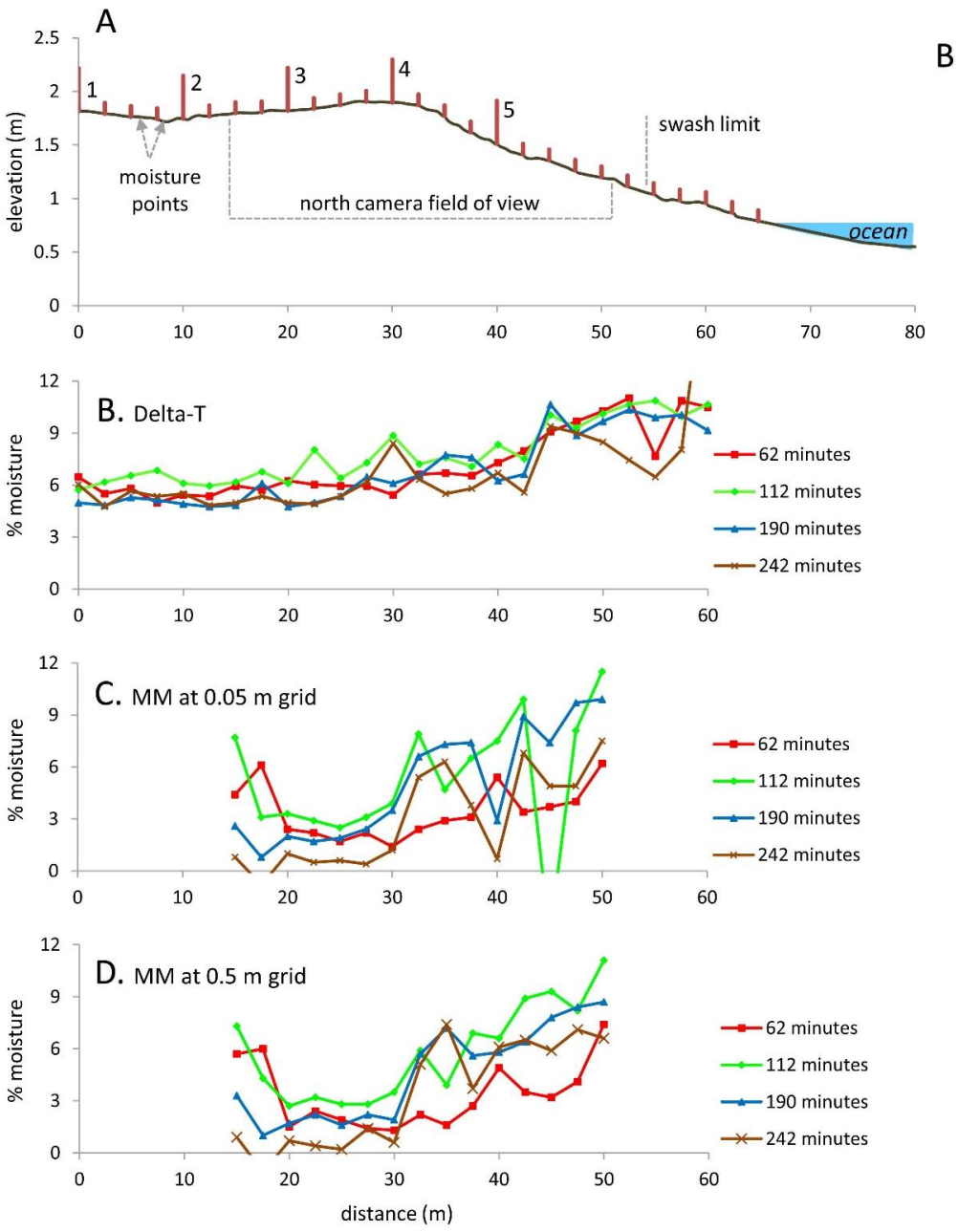


Figure 7: A) Beach profile along the instruments transect; B) Measurements of near surface moisture (upper 2 cm) taken at four times along the instrument profile using the Delta-T Theta Probe; C) Surface moisture at the same four times and locations (within the field of view of the camera) estimated from moisture maps at the original grid resolution of 0.05 m; D) Measurements of surface

moisture from moisture maps at a coarser resolution of 0.5 m.

626

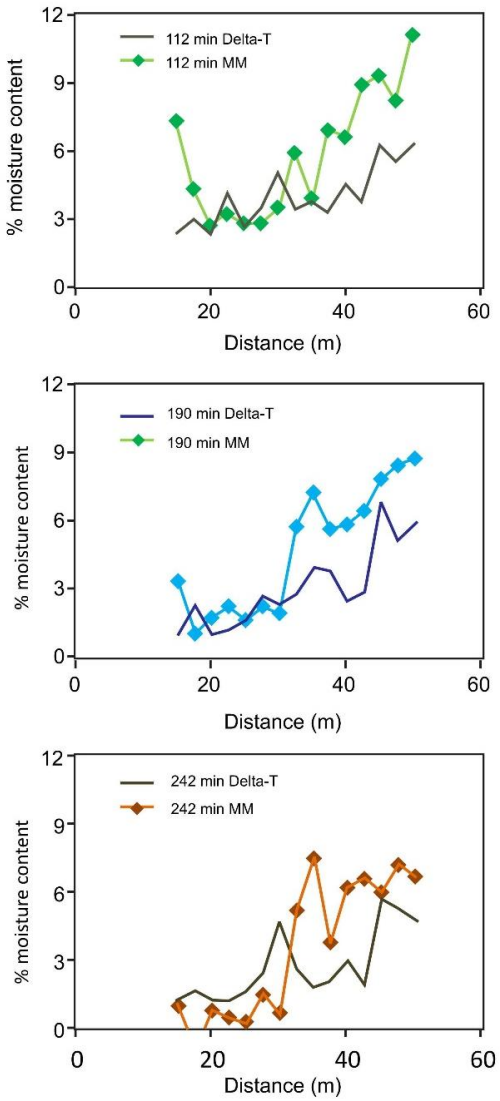


Figure 8: Plot of moisture values from the Delta-T Theta probe and moisture maps (MM) at 0.5 m grid resolution at three different time intervals. In general terms, the MM values show a larger variability of moisture values and sharper differences between the wettest and driest ends.

627

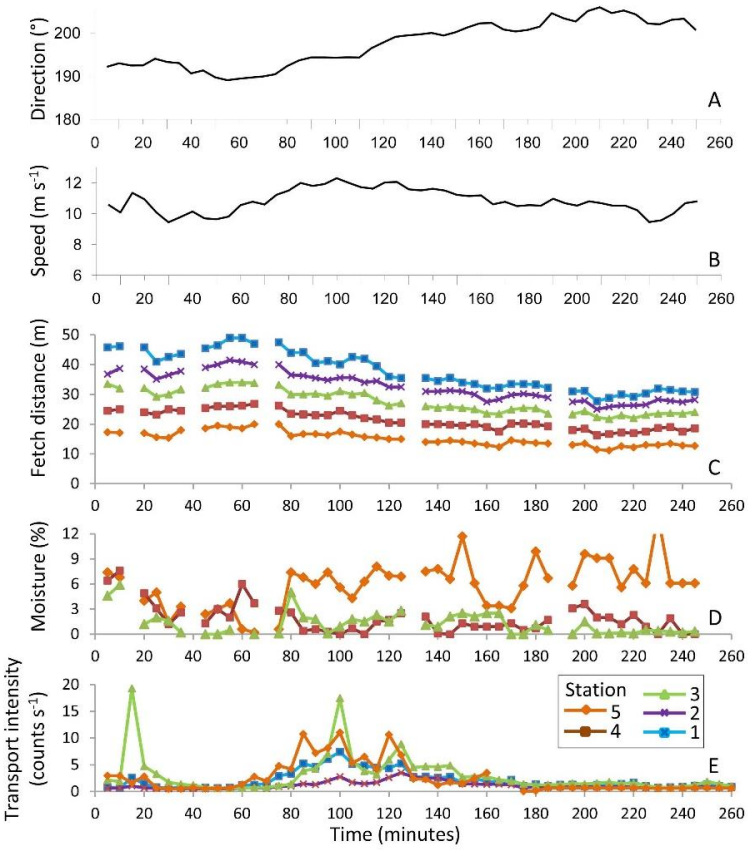


Figure 9: Five minute averages for incident wind direction (A) and wind speed (B) recorded at 3 m high over the beach surface at station 4, fetch distances (C), surface moisture content for stations 3-5 (within the field of view of the camera; D), and sediment transport intensity (E). Gaps in the data correspond to periods of time when no images were taken.

628


Figure 10: Photographs of the beach surface at the end of the transport event: A) close-up of station 4; B) ripples formed in the dry sand accumulation at station 2; C) view of station 4 looking landward showing the eroded and relatively damp surface with a transition to deposition towards station 3 in the background.

629